Journal of Naval Architecture and Marine Engineering
January, 2025
https://dx.doi.org/10.3329/jname.v22i1.78578 http://www.banglajol.info

NUMERICAL EXPLORATION OF MHD NON-NEWTONIAN NANOFLUID FLOW PAST A BIDIRECTIONAL SURFACE WITH RADIATION AND JOULE'S HEAT

T. Jayachandra Reddy[1], B. Ramoorthy Reddy[2], A. Mohanarami Reddy[3]
[1]Dept. of Mathematics, Sri Venkateswara College of Engineering, Tirupati517507, A.P., India.
Email: jayachandrareddy.t@svce.edu.in
[2]Department of H&S, Mother Theresa Institute of Engineering Technology, Palamaner-517408, A.P., India.
Email: ramoorthymaths@gmail.com
[3]Dept. of Mathematics, Sri Venkateswara College of Engineering and Technology, Chittoor-517127, A.P., India.

Abstract:

The present study examines the stimulus of a magnetic field on the three-dimensional movement of Casson nanofluid over a stretchable surface embedded in a porous medium. The belongings of various constraints on the fluid dynamics are also analyzed. The governing nonlinear partial differential equations representing the fluid flow problem are converted into dimensionless ordinary differential equations using similarity transformations. These resulting ODEs are then solved numerically using the R. K. based Shooting method. The impact of various parameters on the flow profiles is illustrated through graphical representations. It is observed that the velocity profile decreases with an increase in the magnetic field number. Moreover, greater radiation parameter values lead to a rise in the distribution of heat and the corresponding layer thickness.

***Keywords*:** Heat and mass transfer, non-Newtonian fluid, MHD, radiation, first order chemical reaction

1. Introduction:

A non-Newtonian fluid is a fluid whose viscosity (resistance to flow) changes depending on the rate of shear strain, or the relative motion between its fluid layers. This behavior contrasts with Newtonian fluids, which maintain a constant viscosity regardless of the shear rate. Non-Newtonian fluids, such as Eyring–Powell fluid, Casson fluid, Prandtl fluid, Reiner–Philipp off fluid, Prandtl–Eyring fluid, Carreau fluid, micropolar fluid, and power-law fluid, have attracted considerable attention from researchers due to their wide range of applications in various industries. Among these, Casson fluid stands out as the most relevant. This fluid is vital in industries like food processing, adhesive and paint manufacturing, nuclear power plant cooling systems, and polymer production. Ali *et al.* (2019) investigated the motion of Casson nanofluid over an elastic sheet. Mabood *et al.* (2020) examined the flow of Casson nanofluid over a flexible surface. Gubena and Ibrahim (2023) studied the flow of Casson nanofluid on an expanding sheet, incorporating a heat flux model. A numerical scrutinization of MHD micropolar fluid flow due to stretching of variable thicked surface in the attendance of dissipation was reported by Kumar *et al.* (2019). The influence Eckert number on MHD micropolar fluid over a bending surface with uneven heat source/sink was reported by Kumar *et al.* (2019) and found an enhancement in fluid temperature for swelling values of non-uniform heat source/sink parameters.

In recent years, the analysis of hydromagnetic flow involving heat and mass transfer in porous medium has attracted the attention of many scholars because of its possible applications in diverse fields of science and technology such as - soil sciences, astrophysics, geophysics, nuclear power reactors, etc. In geophysics, it finds its applications in the design of MHD generators and accelerators, underground water energy storage systems etc. It is worth - mentioning that MHD is now undergoing a stage of great enlargement and differentiation of subject matter. These new problems draw the attention of the researchers due to their varied significance, in liquid metals, electrolytes ionized gases etc. Maleque *et al.* (2005) analyzed the impact of variable properties and Hall current on steady MHD laminar convective fluid flow over a porous rotating disk. Singh (2007) investigated steady MHD free convection and mass transfer flow, incorporating Hall current, viscous dissipation, Joule heating, and the effect of thermal diffusion. Devi *et al.* (2011) explored pulsating convective MHD flow with Hall current, a heat source, and viscous dissipation along a vertical porous plate. Singh *et al.* (2005) examined hydromagnetic free convection and mass transfer flow influenced by Joule heating, thermal diffusion, a heat source, and Hall current. Kumar *et al.* (2024) studied the behavior of nanofluids flowing over a stretchable sheet under the influence of convection.

 Received on: Dec., 2024

Radiation plays a crucial role in many physical phenomena and has significant effects on various processes. Heat energy is transferred through fluid particles via radiation, which is a critical factor in engineering and numerous industrial applications, such as high-temperature operations in fuel pumps, paper plate manufacturing, frozen metal shards, and electronic chips. Consequently, scientists are compelled to study the radiation process, especially when driven by substantial temperature gradients. Researchers have explored radiation effects using diverse flow characteristics. Ahmad *et al.* (2024) investigated the thermal performance of fluid flow through a porous medium, incorporating thermal radiation within a channel between two walls. Albalawi *et al.* (2024) analyzed heat transfer in nanofluid motion around a cylinder, considering the impact of thermal radiation. Ramadevi *et al.* (2019) deliberated the influence of uneven heat source/sink and thermic heat on hybrid nanofluid flow over a bidirectional surface. Aslam *et al.* (2024) studied the effects of thermal radiation on fluid motion within permeable enclosures. Kumar *et al.* (2019) examined the role of heat sink/source on non-Newtonian fluid flow over a wedge. Kempannagari *et al.* (2020) researched the impact of Joule heating on fluid flow over an exponentially stretching sheet.

Chemical reactions play a crucial role in mass and heat transfer studies across academic and technology-driven fields due to their extensive industrial applications. They are essential in processes such as polymer synthesis, designing chemical processing equipment, cooling towers, fog formation, pollution control, dispersion, temperature regulation, and fiber insulation, among others. In industrial chemical operations, raw materials are intentionally subjected to chemical reactions, transforming inexpensive starting materials into high-quality, advanced products. Sandeep *et al.* (2012) have investigated the effect of radiation chemical reaction on transient MHD free convection flow over a vertical plate through a porous medium. Ramadevi *et al.* (2020) have found out the chemical effects on a steady MHD-free convection fluid past a stretched sheet with heat absorption by using the modified heat flux model. Kumar *et al.* (2023) made a study on free convection in MHD nanofluid flow with Heat source. Recently, Rathore *et al.* (2024) examined the flow and heat transfer features of nanofluid flow past a stretching sheet in the presence of radiation.

The literature survey reveals that the combined effects of chemical reactions and electrically conductive MHD have not been extensively studied. This research focuses on the impact of Joule heating, magnetic fields, radiation, heat sources/sinks, and chemical reactions on the three-dimensional flow of Casson nanofluid over a rotating, stretching surface in the presence of porous media. By analyzing how chemical reactions influence flow dynamics, scientists and engineers can enhance the efficiency of heat and mass transfer processes and design systems with optimized flow characteristics. The governing partial differential equations (PDEs) are transformed into dimensionless ordinary differential equations (ODEs) using similarity variables. These ODEs are then solved numerically using the RKF-45 method. The effects of various dimensionless parameters on temperature, velocity, and concentration profiles are illustrated through graphical representations.

2. Formulation:

Let us ponder a steady, 3D, incompressible non-Newtonian nanofluid model subject to borderline conditions from initial to free stream velocity. The classical is electrically conductive, and the exterior is stretchable and penetrable. The velocity of the stretchable surface is $u_w = ax$, here a is the stretching constant. The velocity components are considered as (u,v,w) along (x,y,z) directions. The momentum equation has electric outcome is calculated in the directions of $x-$axis and $y-$axis, as shown in Fig. 1. The temperature distribution is dominated by thermal radiation and heat generation/absorption. The occurrence of higher-order chemical reactions is also considered.

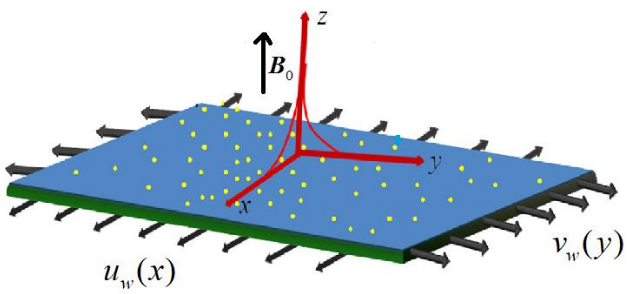

Fig. 1: Geometry of flow problem.

The governing equations are:

$$\frac{\partial v}{\partial y}+\frac{\partial u}{\partial x}+\frac{\partial w}{\partial z}=0 \tag{1}$$

$$u\frac{\partial u}{\partial x}+w\frac{\partial u}{\partial z}+v\frac{\partial u}{\partial y}=\nu_{nf}\left(1+\frac{1}{\beta}\right)\frac{\partial^2 u}{\partial z^2}-\frac{\nu_{nf}}{K^*}u-\frac{\sigma_{nf}}{\rho_{nf}}\beta_0^2 u \tag{2}$$

$$u\frac{\partial v}{\partial x}+w\frac{\partial v}{\partial z}+v\frac{\partial v}{\partial y}=\nu_{nf}\left(1+\frac{1}{\beta}\right)\frac{\partial^2 v}{\partial z^2}-\frac{\nu_{nf}}{K^*}v-\frac{\sigma_{nf}}{\rho_{nf}}\beta_0^2 v \tag{3}$$

$$u\frac{\partial T}{\partial x}+w\frac{\partial T}{\partial z}+v\frac{\partial T}{\partial y}=\alpha_{nf}\frac{\partial^2 T}{\partial z^2}+\frac{\sigma_{nf}}{(\rho C_p)_{nf}}\left[(u+v)\beta_0\right]^2+\frac{Q_0}{(\rho C_p)_{nf}}(T-T_\infty)-\frac{1}{(\rho C_p)_{nf}}\frac{\partial q_r}{\partial z} \tag{4}$$

$$u\frac{\partial C}{\partial x}+w\frac{\partial C}{\partial z}+v\frac{\partial C}{\partial y}=D\frac{\partial^2 T}{\partial z^2}-K_n\left(C-C_\infty\right) \tag{5}$$

The subjected boundary conditions are

$$\left.\begin{array}{ll} u=u_w=ax,\ v=0,\ -k_{nf}\dfrac{\partial T}{\partial z}=h_f(T_f-T),\ C\to C_w,\ w=0, & at\ \ z=0 \\ w\to 0,\ u\to 0,\ v\to 0,\ T\to T_\infty, C\to C_\infty & as\ \ z\to\infty \end{array}\right\} \tag{6}$$

The Rosseland approximation is applied for radiative heat flux as,

$$q_r=-\frac{4\sigma^*}{3K^*}\frac{\partial T^4}{\partial z} \tag{7}$$

Here, the Stefan-Boltzman constant is σ^* and the mean absorption coefficient is expressed as k^*.
Consider the similarity transformations

$$\xi=\sqrt{\frac{a}{\nu_f}}\,z,\ u=axF'(\xi), v=axg(\xi), w=-(a\nu_f)^{1/2}F(\xi), T=T_\infty[1+(\varepsilon-1)\theta(\xi)] \tag{8}$$

The temperature ratio parameter is $\varepsilon=T_f/T_\infty$.

The nanofluid terms are

$$\begin{gathered}\mu_{nf}=\frac{\mu_f}{(1-\phi)^{2.5}},\rho_{nf}=(1-\phi)\rho_f+\phi\rho_s,(\rho c_p)_{nf}=(1-\phi)(\rho c_p)_f+\phi(\rho c_p)_s,\sigma=\frac{\sigma_s}{\sigma_f},\\ \sigma_{nf}=\sigma_f\left[1+\frac{3(\sigma-1)\phi}{(\sigma+2)-(\sigma-1)\phi}\right],k_{nf}=k_f\left[\frac{k_s+2k_f-2\phi(k_f-k_s)}{k_s+2k_f+\phi(k_f-k_s)}\right],\alpha_{nf}=\frac{k_{nf}}{(\rho c_p)_{nf}}.\end{gathered} \tag{9}$$

Utilizing equation (8), the equations (2) – (6) becomes,

$$\Phi_2\left(1+\frac{1}{\beta}\right)F'''+\Phi_1\left(-F_1F'^2+FF''-F'^2\right)+\Phi_3 Ha^2F'-\Phi_2K_1F'=0 \tag{10}$$

$$\Phi_2\left(1+\frac{1}{\beta}\right)g''-\Phi_1\left(F'g-Fg'-F_1g\right)+\Phi_3 Ha^2g'-\Phi_2K_1g=0 \tag{11}$$

$$\begin{gathered}\frac{1}{\Pr}\left\{\Phi_5\theta''+4Ra\left[1+\theta(\varepsilon-1)^2\right](\varepsilon-1)\theta'^2+\frac{4}{3}Ra(1+\theta(\varepsilon-1))^3\theta''\right\}+\\ \left[\Phi_4F\theta'+Ha^2Ec\Phi_3\left[(F'+g)\right]^2\right]+\delta\theta=0\end{gathered} \tag{12}$$

$$\frac{1}{Sc}\phi''+\phi'F-\gamma\phi=0 \tag{13}$$

The associated non-dimensional borderlines are

$$\left.\begin{array}{l} F(\xi)=0,\ F'(\xi)=1, -\Phi_5\,\theta'(\xi)=Bi(1-\theta(\xi)), g(\xi)=0,\ \phi(\xi)=1, at\ \xi=0 \\ F'(\xi)\to 0,\ g(\xi)\to 0,\ \theta(\xi)\to 0, \phi(\xi)\to 0 \qquad as\ \ \xi\to\infty \end{array}\right\} \tag{14}$$

Here

$$\Phi_1=(1-\phi)+\phi(\rho_s/\rho_f),\ \Phi_2=(1-\phi)^{-2.5}, \Phi_3=1+\frac{3(\sigma-1)\phi}{(\sigma+2)-(\sigma-1)\phi}, \Phi_4=(1-\phi)+\phi\frac{(\rho c_p)_s}{(\rho c_p)_f},\ \Phi_5=\frac{k_{nf}}{k_f},$$

Here $K_1=\dfrac{\nu_f}{K^* a}$ is the porous parameter, $Ha^2=\dfrac{\sigma_f B_0^2}{a\rho_f}$ the magnetic parameter, $Ra=\dfrac{4\sigma^* T_\infty^3}{k_f k^*}$ the radiation parameter, $\Pr=\dfrac{(\mu C_p)_f}{k_f}$ is the Prandtl number, $Ec=\dfrac{a^2x^2}{(C_p)_f(T_f-T_\infty)}$ is the Eckert number, $\delta=\dfrac{Q_0}{a(\rho C_p)_f}$ is the heat generation/absorption parameter, and $Bi=\dfrac{h_f}{k_f}\sqrt{\dfrac{\nu_f}{a}}$ is the Biot number is $Bi=\dfrac{h_f}{k_f}\sqrt{\dfrac{\nu_f}{a}}$.

The physical quantities are obtained as follows,

The non-dimensional skin friction coefficients (C_{fx}, C_{fy}) , local Nusselt number (Nu_x) and Sherwood numbers are:

$$\left.\begin{array}{l} C_{fx}\left(\mathrm{Re}_x\right)^{1/2}=A_2\left(1+\dfrac{1}{\beta}\right)F''(0), C_{fy}\left(\mathrm{Re}_x\right)^{1/2}=A_2\left(1+\dfrac{1}{\beta}\right)g'(0), \\ Nu_x\left(\mathrm{Re}_x\right)^{-1/2}=-\left[\Phi_5+\dfrac{4}{3}Ra\left\{1+(\varepsilon-1)\theta(0)\right\}^3\right]\theta'(0), Sh_x\left(\mathrm{Re}_x\right)^{-1/2}=-\phi'(0), \end{array}\right\} \tag{15}$$

Here $\mathrm{Re}_x=\dfrac{xu_w}{\nu_f}$ stands for local Reynolds number.

3. Results and Discussion:

This section details the computational methodology. Equations (10)-(14) demonstrate both nonlinearity and interdependence. By utilizing similarity transformations, the partial differential governing equations are converted into nonlinear algebraic equations. These transformed equations are subsequently substituted into the system for further analysis. It is thus recommended to address these equations through a numerical technique. Numerical solutions for the boundary value problem (BVP) must be obtained using the RKF-45 method algorithm. Initially, to accomplish this objective, transform the BVP into an initial value problem (IVP) with specified starting conditions. The physical clarification of each dimensionless parameters in momentum (F'), energy (θ) and concentration (ϕ) are focused by fixing other constraints and assign to them some fixed input values such as $Ha=2,\ n=1, K_1=1, F_1=0.2, Ra=0.3, \delta=0.3,\ \beta=0.2, \gamma=0.1, Bi=1.5,,\ Ec=1, \Pr=7,$ $Sc=1.2, \Phi_1=0.6, \Phi_2=0.6, \Phi_4=0.4, \Phi_5=0.4$. The thermo physical values of the base fluid and nanoparticle are shown in Table 1.

Table 1: The thermo physical properties are

	$\rho\left(kgm^{-1}\right)$	$k\left(Wm^{-1}K^{-1}\right)$	$C_p\left(Jkg^{-1}K^{-1}\right)$	$\sigma\left(Sm^{-1}\right)$
Base fluid	1060	0.505	8933	1.07×10^{-4}
$MnFe_2O_4$	4870	0.67	130	120×10^{6}

Figs. 2-4 display the geometrical representation of magnetic constraints for larger values on $F'(\xi), \theta(\xi) \& \phi(\xi)$. A noteworthy reduction in these outlines is detected with a higher slope gradient variation. This is due to the consequence of drag force in the porous medium. It is detected from Fig. 3 and 4, that the energy and concentration distribution is boosted for higher magnetic parameter values. Fig. 5 portrays the consequence of Ra on $\theta(\xi)$. Graphs reveal that intensification in radiation parameter enhances the temperature distribution.

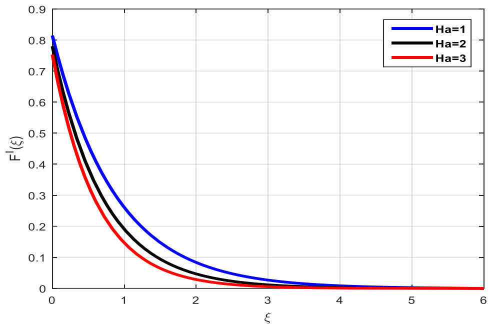

Fig. 2. Stimulus of Ha on $F'(\xi)$.

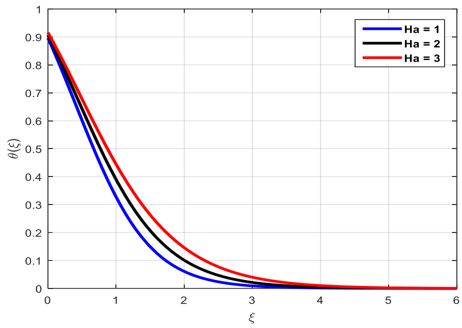

Fig. 3. Stimulus of Ha on $\theta(\xi)$

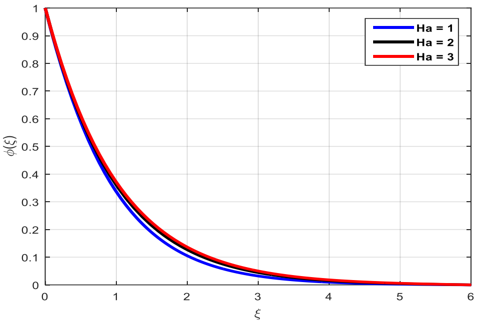

Fig. 4. Stimulus of Ha on $\phi(\xi)$

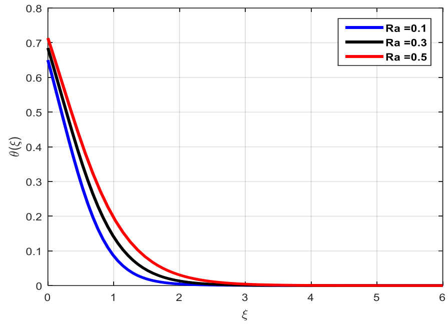

Fig. 5. Stimulus of Ra on $\theta(\xi)$

Fig. 6 is sketched to evaluate the performance of the nature of the porosity parameter on the velocity. The increase in K_1 declines the $F'(\xi)$. The reason behind this is magnetic strength and porous medium. The effect of δ on the distribution of heat is depicted in Fig. 7. The rise in δ intensifies the curves of heat. The heat movement within the system will accelerate as heat source levels climb. The heat sink will function as an exchanger, transferring heat from the external environment into the nanofluid.

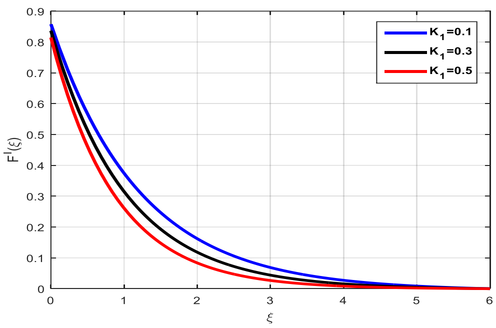

Fig. 6. Stimulus of K_1 on $F'(\xi)$

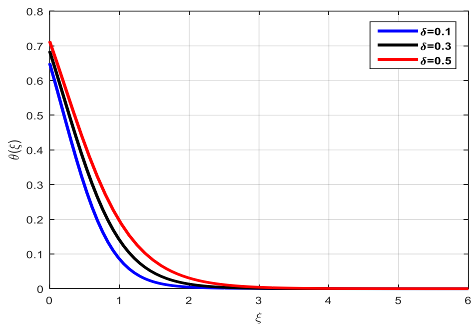

Fig. 7. Stimulus of δ on $\theta(\xi)$

The effect of γ on the heat is depicted in Fig. 8. The disparities lead to a decay in the $\phi(\xi)$ for more values of chemical reaction parameter. The nano-fluid particles in the strained surface are the purpose for the decline of species gradient in the permeable medium. The impact of Eckert number is sketched in Fig. 9 to encounter temperature distribution. Automatic energy is derived from thermal energy in energy distribution pertaining to viscous dissipation. It is noted that augmenting Ec less forces acted in the viscous dissipation of temperature distribution. Due to impact of heat generation dominations led Eckert's number to enhance to higher values.

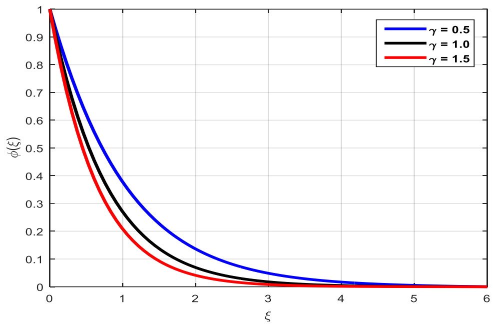

Fig. 8. Stimulus of γ on $\theta(\xi)$

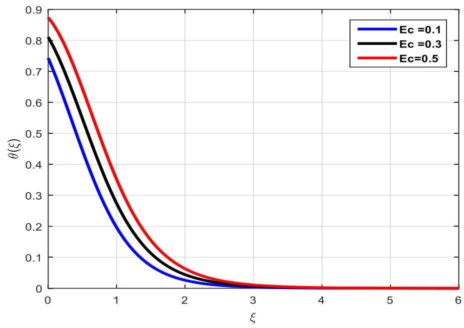

Fig. 9. Stimulus of Ec on $\theta(\xi)$

The impact of Biot number is sketched in Fig. 10 to encounter temperature distribution. It is noted that augmenting Bi causes an enactment in the temperature distribution. Figure 11 is portrayed to analyse the impact of Schmidt number (Sc) on concentration. By increasing values of Schmidt number decreases the fluid concentration. Actually, Schmidt number is the ratio of momentum diffusivity and mass diffusivity. Hence, the distribution of concentration and the corresponding layer thickness decreases for increasing values of Schmidt number.

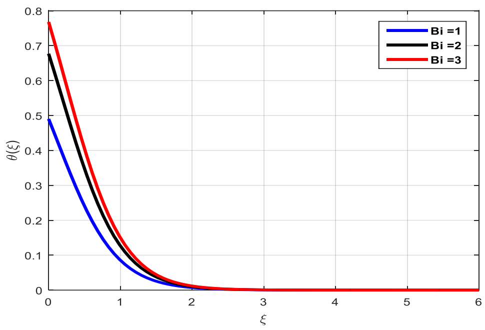

Fig. 10. Stimulus of Bi on $\theta(\xi)$

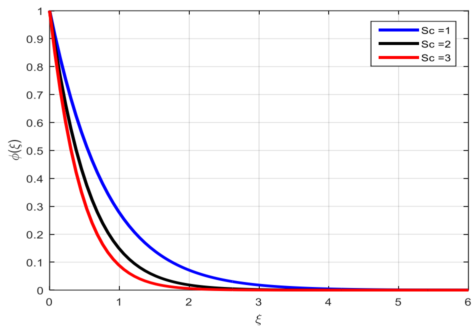

Fig. 11. Stimulus of Sc on $\phi(\xi)$

4. Conclusions

A steady, three-dimensional magnetohydrodynamic flow of Casson fluid over a stretching sheet is studied in the presence of a porous medium. With the aid of appropriate similarity variables, the governing PDEs are transformed into ODEs which are solved numerically using the RKF method. The following is a list of some of the study's key findings based on the above mentioned results and discussion:

- A decrease in the distribution of velocity is detected for increasing values of magnetic field and porosity parameter.
- Concentration profile falls for growing value of Schmidt number and chemical reaction constraint.
- Temperature is a swelling factor of radiation and variable heat source/sink constraints.
- It is perceived that increasing values of solutal slip parameter reduces the distribution of concentration.
- The improvement in the distribution of heat can be seen as the Biot number upsurges.

References

Ali, L., Liu, X., Ali, B., Mujeed, S., and Abdal, S. (2019): Finite element analysis of thermo-diffusion and multi-slip effects on MHD unsteady flow of Casson nano-fluid over a shrinking/stretching sheet with radiation and heat source. Applied Sciences, 9(23), 5217.
https://dx.doi.org/10.3329/jname.v21i1.7039610.3390/app9235217.

Mabood, F., Ibrahim, S. M., Kumar, P. V., and Lorenzini, G. (2020): Effects of slip and radiation on convective MHD Casson nanofluid flow over a stretching sheet influenced by variable viscosity. Journal of Engineering Thermophysics, 29, 303-315. https://dx.doi.org/10.3329/jname.v21i1.7039610.1134/S1810232820020125.

Gubena, T., and Ibrahim, W. (2023): A 3D flow analysis of Casson Nano-fluid flow over a stretching surface with non-Fourier heat and non-Fick's mass flux. International Journal of Thermofluids, 20, 100488. https://dx.doi.org/10.3329/jname.v21i1.7039610.1016/j.ijft.2023.100488.
Anantha Kumar, K., Sugunamma, V., and Sandeep, N. (2020): Influence of viscous dissipation on MHD flow of micropolar fluid over a slendering stretching surface with modified heat flux model. Journal of Thermal Analysis and Calorimetry, 139, 3661-3674. https://dx.doi.org/10.1007/s10973-019-08694-8.
Kumar, A., Sugunamma, V., and Sandeep, N. (2019): Numerical exploration of MHD radiative micropolar liquid flow driven by stretching sheet with primary slip: a comparative study. Journal of Non-Equilibrium Thermodynamics, 44(2), 101-122. https://dx.doi.org/10.1515/jnet-2018-0069.
Maleque, K. A., and Sattar, M. A. (2005): The effects of variable properties and Hall current on steady MHD laminar convective fluid flow due to a porous rotating disk. International Journal of Heat and Mass Transfer, Vol. 48, pp. 4460-4466. https://dx.doi.org/10.1016/j.ijheatmasstransfer.2005.05.017 .
Singh, A. K. (2003): MHD free convection and mass transfer flow with Hall current, viscous dissipation, Joule heating and thermal diffusion. Indian Journal of Pure and Applied Physics, Vol. 41, pp. 24-35. http://nopr.niscpr.res.in/handle/123456789/25026.
Anjali Devi, S. P., Shailendhra, K., and Hemamalini, P. T., (2011): Pulsated convective MHD flow with Hall current, heat source and viscous dissipation along a vertical porous plate. International Journal of Applied Mathematics and Computation, Vol. 3 (2), pp. 141-150, 2011. https://dx.doi.org/10.0000/ijamc.2011.3.2.137.
Singh, A. K., Singh, A. K., and Singh, N. P. (2005): Hydromagnetic free convection and mass transfer flow with Joule heating, thermal diffusion, heat source and Hall current. Bulletin-Institute of Mathematics Academia Sinica, 33(3), 291.
Kumar, K. A. (2024): A computational model for the density of motile micro-organisms in the Casson fluid flow with thermal radition: Journal of Naval Architecture and Marine Engineering, 21(1), 79-86. https://dx.doi.org/10.3329/jname.v21i1.70396.
Ahmad, B., Abbas, T., Fatima, K., Duraihem, F. Z., and Saleem, S. (2024). Nonlinear flow of hybrid nanofluid with thermal radiation: A numerical investigation. ZAMM‐Journal of Applied Mathematics and Mechanics/Zeitschrift für Angewandte Mathematik und Mechanik, 104(1), e202200170. https://dx.doi.org/10.1002/zamm.202200170.
Saad Albalawi, K., Karthik, K., Madhu, J., Bin-Asfour, M., Alkahtani, B. S. T., Alazman, I., and Kumar, R. N. (2025): Nanoparticle aggregation kinematics and nanofluid flow in convectively heated outer stationary and inner stretched coaxial cylinders: Influenced by linear, nonlinear, and quadratic thermal radiation. Modern Physics Letters B, 39(01), 2450361. https://dx.doi.org/10.1142/S0217984924503615.
Ramadevi, B., Kumar, K. A., Sugunamma, V., and Sandeep, N. (2019): Influence of non-uniform heat source/sink on the three-dimensional magnetohydrodynamic Carreau fluid flow past a stretching surface with modified Fourier's law. Pramana, 93, 1-11. https://dx.doi.org/10.1007/s12043-019-1847-7.
Aslam, M. A., Yao, H., Shahzad, H., Algarni, S., Alqahtani, T., and Irshad, K. (2024): Impact of thermal radiation in a mixed convective magnetize Casson fluid flow through a porous bulb-shaped enclosure. Journal of Thermal Analysis and Calorimetry, 1-13. https://dx.doi.org/10.1007/s10973-024-13048-0.
Kumar, K. A., Ramadevi, B., Sugunamma, V., and Reddy, J. R. (2019): Heat transfer characteristics on MHD Powell-Eyring fluid flow across a shrinking wedge with non-uniform heat source/sink. Journal of Mechanical Engineering and Sciences, 13(1), 4558-4574. https://dx.doi.org/10.15282/jmes.13.1.2019.15.0385.
Kempannagari, A. K., Buruju, R. R., Naramgari, S., and Vangala, S. (2020): Effect of Joule heating on MHD non‐Newtonian fluid flow past an exponentially stretching curved surface. Heat Transfer, 49(6), 3575-3592. https://dx.doi.org/10.1002/htj.21789.
Sandeep, N., Reddy, A. V. B., and Sugunamma, V. (2012): Effect of radiation and chemical reaction on transient MHD free convective flow over a vertical plate through porous media. Chemical and process engineering research, 2, 1-9.
Ramadevi, B., Anantha Kumar, K., Sugunamma, V., Ramana Reddy, J. V., and Sandeep, N. (2020). Magnetohydrodynamic mixed convective flow of micropolar fluid past a stretching surface using modified Fourier's heat flux model. Journal of Thermal Analysis and Calorimetry, 139, 1379-1393. https://dx.doi.org/10.1007/s10973-019-08477-1.
Anantha Kumar, K., Sandeep, N., Samrat, S. P., and Ashwinkumar, G. P. (2023): Effect of electromagnetic induction on the heat transmission in engine oil-based hybrid nano and ferrofluids: A nanotechnology application. Proceedings of the Institution of Mechanical Engineers, Part E: Journal of Process Mechanical Engineering, 237(6), 2488-2495. https://dx.doi.org/10.1177/09544089221139569.
Rathore, N., Kumar, K. A., and Sandeep, N. (2024): Analysis of nanomodels for nanofluid flow over a curved region with MXene (Ti3C2). Journal of Thermal Analysis and Calorimetry, 1-8. https://dx.doi.org/10.1007/s10973-024-13916-9.